Green Intelligent Systems and Applications

Research Article
Volume 6(1), 2026, 34–50
https://doi.org/10.53623/gisa.v6i1.1012

Design and Implementation of a Multi-Node Gas Sensor-Based Indoor Air Quality Monitoring and Control System

Siti Milda Alkan Dawasoka*, Eka Puji Widiyanto

Faculty of Computer Science and Engineering, Multi Data Palembang University, Palembang, Indonesia

*Correspondence: sitimildaalkandawasoka_2226270025@mhs.mdp.ac.id

SUBMITTED: 25 January 2026; REVISED: 14 February 2026; ACCEPTED: 19 February 2026

ABSTRACT: Air quality monitoring was a crucial aspect of maintaining occupational health and safety, particularly in industrial environments. This study proposed the design and implementation of an Internet of Things (IoT)-based indoor air quality monitoring system capable of measuring environmental parameters in real time. The system integrated an ENS160 gas sensor and an AHT21 temperature–humidity sensor with a Wemos D1 Mini microcontroller. Sensor data were transmitted via the MQTT protocol to an Orange Pi 4A server and visualized using a Node-RED dashboard. The monitored parameters included Total Volatile Organic Compounds (TVOC), equivalent CO_2 (eCO_2), temperature, and humidity. Experimental evaluation demonstrated that the system responded proportionally to different pollutant exposure levels. Under high NH_3 exposure (100%), TVOC values reached a maximum of 12,697 ppb with an average of 5,037 ppb, clearly exceeding the hazardous threshold (>200 ppb). At moderate exposure (50%), the average TVOC decreased to 2,106 ppb, while at low exposure (10%), the average value remained within the safe range at 84 ppb. For eCO_2 testing, cigarette smoke exposure produced a peak value of 11,524 ppm with an average of 1,663 ppm, indicating hazardous conditions (>1000 ppm). Statistical analysis using mean and standard deviation confirmed that sensor stability improved at lower pollutant concentrations. The proposed system successfully provided stable real-time monitoring, threshold-based classification, and automatic mitigation control, demonstrating its feasibility for intelligent indoor air quality management in industrial workspaces.

KEYWORDS: Indoor air quality; internet of things; ENS160 sensor; multi-node monitoring system; real-time air pollution detection

1. Introduction

Clean and comfortable air is a basic necessity for human health and productivity. However, approximately 99% of the world's population still breathed air with pollution levels exceeding safe limits [1]. Exposure to air pollutants generated by industrial chemical activities could trigger respiratory disorders, cause irritation, and reduce work performance. In Indonesia, air pollution remained a serious issue, with industrial activities, transportation, and biomass

burning identified as major contributors of pollutants such as particulate matter ($PM_{2.5}$/PM_{10}), harmful gases, and chemical compounds that increased the risk of respiratory and cardiovascular diseases [2]. Therefore, effective air quality monitoring and management, particularly in occupational and industrial environments, was essential to protect workers' health and safety.

Indoor air quality (IAQ) played a significant role in determining human health and comfort, as most daily activities were performed indoors. Continuous exposure to indoor pollutants has been associated with chronic respiratory and cardiovascular diseases, emphasizing the importance of continuous and reliable monitoring systems [3]. Recent technological developments showed that Internet of Things (IoT)-based IAQ monitoring systems enabled real-time environmental data acquisition and integration with centralized monitoring platforms [4]. The integration of IoT architectures with advanced sensing technologies further improved scalability, remote accessibility, and environmental data processing capabilities in modern monitoring systems [5].

Several studies demonstrated practical implementations of IoT-based air quality monitoring. Rahmadani et al. developed a real-time monitoring system integrated with web-based visualization for campus environments [6], while Azizah et al. implemented an IoT monitoring system equipped with automatic notification features when pollutant thresholds were exceeded [7]. Distributed monitoring platforms using MQTT and Node-RED architectures were also explored for multi-point environmental monitoring applications [8]. In industrial contexts, intelligent control strategies such as ANFIS-based VOC mitigation systems were proposed to improve emission control effectiveness [9].

This study was conducted in a large-scale fertilizer manufacturing environment that utilized chemical substances, including ammonia (NH_3), as part of its production processes. Controlling gaseous emissions, particularly ammonia, was essential because prolonged exposure could pose health risks and reduce workplace comfort [10]. In addition, carbon dioxide (CO_2) was an important parameter in IAQ assessment, as prolonged exposure to moderate CO_2 concentrations could reduce alertness and cognitive performance [11], while short-term exposure might cause mild irritation and respiratory discomfort [12].

Although numerous IoT-based air quality monitoring systems had been developed, many existing implementations remained limited to single-node measurements, relied on analog gas sensors, or primarily focused on visualization and notification features without integrating scalable multi-node architectures and automatic mitigation mechanisms [13–15]. Moreover, low-cost gas sensors were often sensitive to environmental variations, potentially affecting measurement stability and reliability [16,17]. Therefore, a scalable multi-node IAQ monitoring system capable of distributed sensing, real-time data processing, and automatic environmental control was still required.

In this study, digital environmental sensing modules were employed to monitor gas parameters, temperature, and humidity, enabling stable real-time indoor air quality measurements. Unlike many previous systems that primarily focused on monitoring and notification functions, the proposed approach introduced a scalable multi-node indoor monitoring architecture integrated with real-time data acquisition, visualization, threshold-based classification, and automatic exhaust mitigation control. Compared to analog gas sensors, the ENS160 provided digital output, lower power consumption, and improved measurement stability, while the AHT21 sensor enabled environmental compensation for more consistent

readings [18–20]. This study demonstrated the implementation of a multi-node indoor air quality (IAQ) monitoring system capable of real-time sensing, distributed data communication, and automated environmental response, making it suitable for deployment in industrial workplace environments.

2. Materials and Methods

2.1. System architecture and block diagram.

The proposed system consisted of three sensor nodes deployed at different indoor locations. Each node functioned independently to acquire environmental data and transmit the measurements wirelessly to a central gateway. The gateway, implemented using an Orange Pi 4A platform, acted as both an MQTT broker and a data distribution server that forwarded sensor data to the visualization layer. Figure 1 showed the architecture of the multi-node air quality monitoring system, consisting of one main node (Node 1) and two additional nodes (Node 2 and Node 3). Each node used a Wemos D1 Mini microcontroller operating in station (STA) mode as a wireless network client. The microcontroller functioned as a data processing unit and sent data to the central server via the MQTT protocol. On Node 1, the data obtained was processed locally and displayed on a 16×2 LCD. In addition, this node was connected to an actuator module in the form of an exhaust fan that was automatically controlled based on the results of air quality classification. Thus, Node 1 acted not only as a monitoring unit but also as a mitigation unit.

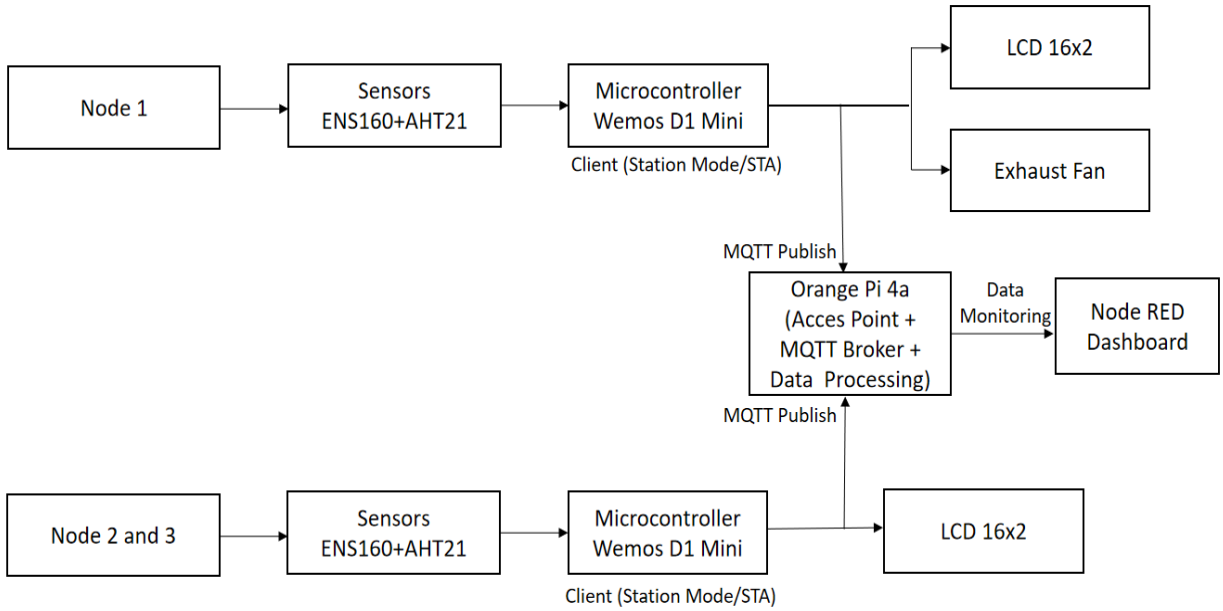

Figure 1. System block diagram.

Node 2 and Node 3 functioned as additional monitoring units placed in different locations within the room. Both nodes displayed data locally via a 16×2 LCD and periodically sent data to the gateway without being equipped with a control actuator. All data from each node was sent via the MQTT publish mechanism to the Orange Pi 4A, which acted as an access point, MQTT broker, and data processing center. The gateway then forwarded the data to the Node-RED dashboard for real-time visualization and monitoring. This architecture enabled the

system to perform distributed monitoring with centralized processing and supported the integration of monitoring and automatic control functions in a single network platform.

2.2. Hardware design (Node 1, Node 2 and 3).

The hardware used in this study was designed to support IoT-based indoor air quality monitoring and control with a multi-node architecture. The system consisted of a main node (Node 1), which functioned as both a monitoring and control unit, and additional nodes (Node 2 and Node 3), which functioned as portable monitoring units (Figure 2).

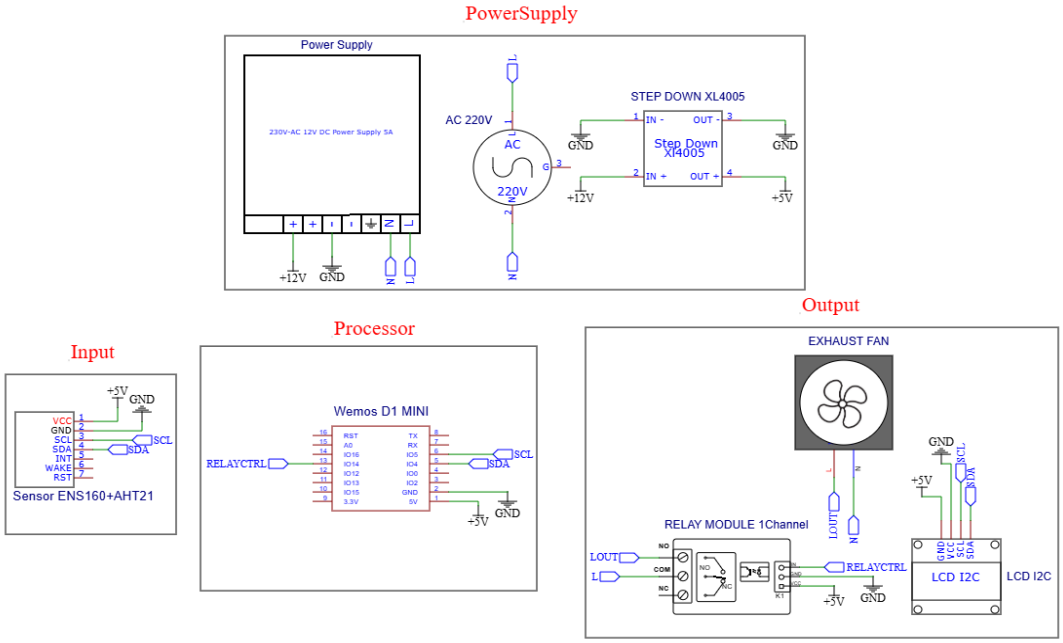

Figure 2. Schematic diagram of node 1 system circuit.

During the development of this system, detailed schematic design was conducted to ensure that all components operated as intended and that the circuit functioned reliably as an integrated unit. The schematic design process verified correct electrical connections, power distribution, and communication pathways between sensors, microcontrollers, displays, and actuators. Table 1 provides a comprehensive overview of the hardware components and power supply configuration used in Node 1, which served as the main monitoring and control unit. The Wemos D1 Mini microcontroller formed the core of the system, handling both data acquisition from the environmental sensors and wireless communication with the central gateway via the MQTT protocol. All low-voltage components, including the ENS160 gas sensor, AHT21 temperature–humidity sensor, and 16×2 LCD module, were supplied with a stable 5 V output generated by an XL4005 step-down converter from a 12 V DC input. To enable automatic mitigation, a relay module controlled by the microcontroller was used to switch a 220 V AC exhaust fan on or off whenever measured pollutant concentrations exceeded predefined threshold values, providing active air quality management. Figure 2 illustrates the circuit schematic for Nodes 2 and 3, which functioned as supplementary monitoring units without actuator control but maintained the same data acquisition and wireless transmission capabilities. This design ensured consistent monitoring across multiple locations while enabling centralized control and visualization of indoor air quality.

Table 1. Hardware components and power supply configuration.

No	Component	Function	Operating Voltage	Power Source
1	Wemos D1 Mini	Main controller for data acquisition and communication	5 V (via USB) / 3.3 V logic	XL4005 Step-Down Converter
2	ENS 160+AHT21 Sensors	Detection of TVOC, eCO_2, temperature, and humidity	5 V	XL4005 Step-Down Converter
3	LCD Display	Local visualization of air quality status	5 V	XL4005 Step-Down Converter
4	XL4005 Step-Down Converter	Regulates 12 V input to stable 5 V output	Input: 12 V, Output: 5 V	Power Supply (AC 220 V → DC 12 V)
5	Relay Module	Automatic activation/deactivation of exhaust fan	5 V control	AC 220 V
6	Exhaust Fan	Removes polluted air exceeding threshold limits	220 V AC	External DC input
7	Power Supply	Converts AC 220 V to DC 12 V	Input: 220 V AC, Output: 12 V DC	AC 220 V

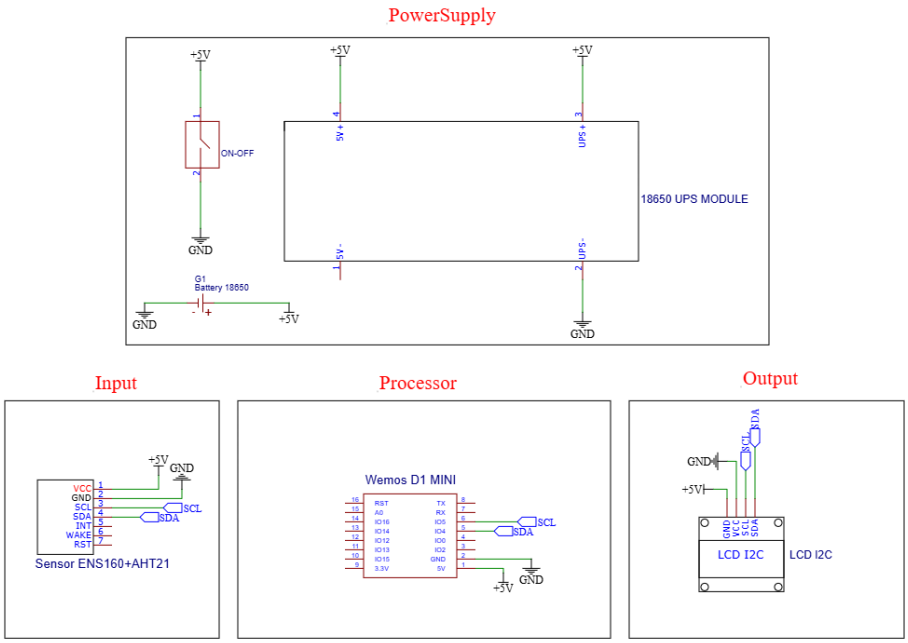

Figure 3. Node 2 and 3 circuit schematic.

Nodes 2 and 3 functioned as portable monitoring units without integrated control actuators, providing flexible deployment for distributed air quality assessment within the room. Similar to the main node, both units utilized the Wemos D1 Mini microcontroller for data processing and MQTT-based wireless communication, as well as the ENS160 and AHT21 sensors to measure environmental parameters including Total Volatile Organic Compounds (TVOC), equivalent CO_2 (eCO_2), temperature, and humidity. Unlike Node 1, these nodes were powered by 18650 lithium-ion batteries with an integrated UPS module, allowing continuous operation and flexible placement without reliance on a direct AC power supply. Sensor readings were displayed locally on a 16×2 I²C LCD for immediate visualization, while simultaneously transmitting data wirelessly to the central Orange Pi 4A gateway using the MQTT protocol. This configuration enabled real-time, multi-point monitoring of indoor air quality across different locations. The complete list of hardware components and their

corresponding power supply configurations for Nodes 2 and 3 is summarized in Table 2, highlighting the integration of battery power, voltage regulation, and sensor interfacing to ensure stable and autonomous operation.

Table 2. Hardware components and power supply configuration.

No	Component	Function	Operating Voltage	Power Supply Configuration
1	Wemos D1 Mini	Data processing and MQTT-based wireless communication	5 V (USB) / 3.3 V logic	Supplied from UPS module (5 V output)
2	ENS160 + AHT21	Measurement of TVOC, eCO_2, temperature, and humidity	3.3 V	Powered via Wemos D1 Mini 3.3 V output
3	LCD 16×2 (I^2C)	Local display of air quality status and environmental parameters	5 V	Supplied from UPS module (5 V output)
4	18650 Lithium Battery	Primary portable energy source	3.7 V nominal	Directly connected to UPS module
5	18650 UPS Module	Battery charging management and voltage regulation (boost to 5 V)	Input: 3.7 V, Output: 5 V	Connected to 18650 battery and AC/DC input
6	AC 220 V Input	External charging source for battery	220 V AC	Supplies UPS charging circuit

2.3. Software Implementation and communication protocols.

This section describes the operational mechanism of the developed air quality monitoring system, including device initialization, data acquisition, wireless communication, and automatic control processes. Each sensor node, based on a Wemos D1 Mini microcontroller, was connected to an Orange Pi 4A gateway, which functioned as an access point and MQTT broker. After successful network initialization, the microcontroller periodically read sensor data and sent it to the server using the MQTT publish–subscribe protocol.

Sensor measurements were collected every 2–3 seconds, resulting in approximately 130 samples during each 5-minute experiment session. Each transmission contained a structured JSON payload that included TVOC (ppb), estimated CO_2 (ppm), temperature (°C), and relative humidity (%RH), with an average message size of approximately 100–150 bytes, ensuring lightweight communication suitable for real-time IoT applications. Received data were processed and displayed via a Node-RED dashboard for real-time monitoring, while key parameters were also shown locally on an LCD module. Operating within a local area network (LAN), the system experienced minimal communication latency and no significant packet loss during testing, enabling reliable real-time visualization and threshold-based actuator control.

Figure 4 illustrates the operational workflow of the proposed system. After initializing the microcontroller and sensors, the device established a WiFi connection and connected to the MQTT broker hosted on the Orange Pi 4A. Sensor data were collected at periodic intervals and transmitted to the dashboard for visualization. The system then evaluated whether the measured TVOC value exceeded 200 ppb or the estimated CO_2 exceeded 1000 ppm. If either threshold was exceeded, the system classified the condition as “Danger,” activated the ventilation fan, and updated the dashboard status. Otherwise, the condition was classified as “Safe,” and the

fan remained inactive. The monitoring process ran continuously in a loop to ensure real-time environmental assessment and automatic mitigation (Figure 4).

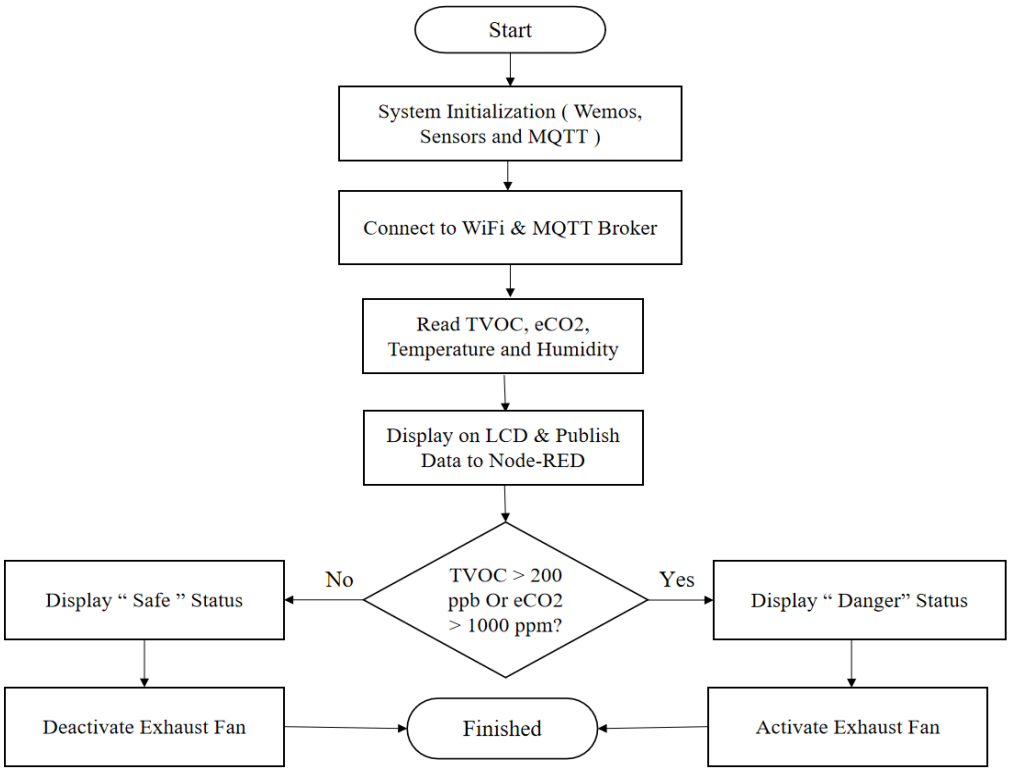

Figure 4. System operation flowchart.

The Node-RED flowchart illustrates the data handling and visualization process on the server side (Figure 5). Data from each sensor node were received through the MQTT subscription node and then processed using the JSON parsing component to extract relevant parameters. Each parameter, including TVOC, eCO_2, temperature, and humidity, was directed to specific dashboard elements such as gauges, graphs, and numeric indicators, enabling real-time monitoring and trend observation over time. In addition to visualization, the flow incorporated functional nodes responsible for evaluating air quality thresholds. When pollutant levels exceeded predetermined values, the system generated a warning status and sent a control signal to activate the exhaust fan. This real-time feedback loop ensured timely mitigation in response to hazardous air quality conditions. The modular structure of Node-RED allowed for flexible expansion, supporting the addition of new sensor nodes, different environmental parameters, or alternative control strategies without requiring significant modifications to the overall architecture. Figure 5 shows the design of the Node-RED website dashboard, highlighting the visualization of environmental parameters, threshold indicators, and real-time status updates for each monitoring node.

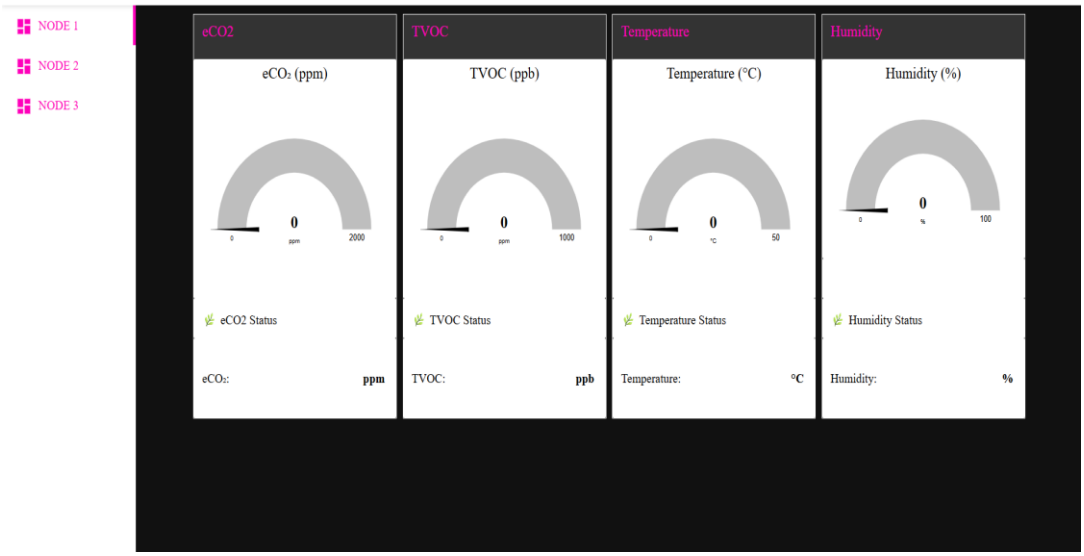

Figure 5. Node-RED website dashboard design.

2.4. Experimental procedure and data acquisition.

System testing was conducted to evaluate the sensors' response to variations in pollutant exposure within a semi-enclosed space. The test environment consisted of a laboratory room with a volume of approximately 36 m³ (3 m × 4 m × 3 m). During the experiments, the doors and windows were closed, and no mechanical ventilation was used to ensure stable pollutant concentrations within the test chamber. The sensors were positioned at a distance of approximately 20 cm from the pollutant source, avoiding direct contact with the test liquid or material. Each test session lasted approximately five minutes, with periodic readings taken at short intervals, resulting in roughly 130 data samples per experiment. The collected data included Total Volatile Organic Compounds (TVOC), estimated CO_2 (eCO_2), temperature, and relative humidity, providing a comprehensive view of the indoor air quality conditions.

The tests were conducted under two main schemes. The first scheme evaluated the sensors' TVOC response to NH_3 solution at concentrations of 100%, 50%, and 10%, with the solution placed near the sensor to observe variations in response due to increasing ammonia-based volatile compounds. The second scheme assessed the eCO_2 response to typical indoor VOC sources, specifically cigarette smoke and air fresheners, chosen because they reflect common real-world indoor pollutants.

All sensor readings were transmitted in real time using the MQTT protocol to the Orange Pi 4A server and stored in a MySQL database for further analysis. The stored data were then exported and processed to calculate the mean and standard deviation, which served as indicators of measurement trends, sensor reliability, and overall system stability during operation.

2.5. Performance evaluation.

System performance was evaluated based on three main aspects: sensor response to concentration variations, measurement stability, and threshold-based classification capability.

2.5.1. Concentration response evaluation.

Sensor response was assessed by analyzing changes in TVOC and eCO_2 values as pollutant concentrations increased. Performance was considered satisfactory if the sensors exhibited a proportional increase in measured values corresponding to the intensity of exposure. This relationship was examined by comparing the minimum, maximum, and average values obtained in each test scenario, providing insight into the sensors' sensitivity and responsiveness.

2.5.2. Measurement stability evaluation.

Measurement stability was evaluated to determine the consistency and reliability of sensor readings throughout the experimental period. Statistical parameters, including the mean and standard deviation, were used to quantify central tendency and dispersion of the data, following standard statistical analysis methods [21]. This evaluation allowed for the identification of fluctuations or drift in sensor output under controlled testing conditions, ensuring the robustness of the monitoring system.

$$\bar{x} = \sum \frac{x_i}{N}$$

$$\sigma = \sqrt{\sum \frac{(X_i - \mu)2}{N}}$$

The average value of the measurements was calculated to represent the central tendency of the collected data. In this calculation, $X_i$represented each individual measurement, while Ndenoted the total number of samples. The standard deviation was calculated to quantify the dispersion of the data around the mean. In this calculation, $X_i$represented each measurement value, Ndenoted the total number of samples, $\mu$was the mean value, and σrepresented the standard deviation. These statistical parameters were used to evaluate the consistency and stability of the sensor measurements throughout the experiments.

The mean value indicates the general concentration trend, while the standard deviation reflects measurement stability and response variability. The mean value represents the overall concentration trend of the measured parameter during each test session, while the standard deviation reflects the variability and stability of the sensor response. A smaller standard deviation indicates more stable measurements, which indicates consistent sensor performance under controlled environmental conditions. Conversely, a larger standard deviation implies a higher level of fluctuation, which may be caused by rapid pollutant accumulation, transient sensor behavior, or environmental disturbances.

2.5.3. Threshold classification evaluation.

A threshold classification evaluation was conducted to determine the system's ability to identify indoor air quality conditions based on applicable regulatory standards. This study referred to the Indonesian Minister of Health Regulation No. 1077/MENKES/PER/V/2011, which classifies indoor air quality into two categories: Safe Threshold and Danger Threshold [13]. The threshold values used in this study are summarized in Table 3. For the TVOC parameter, values below 200 ppb were categorized as safe, while values in the range of 200–

500 ppb were classified as dangerous. For the eCO_2 parameter, values below 1000 ppm were considered safe, whereas values between 1000 and 1500 ppm were classified as dangerous. The use of these national regulations was chosen because they are directly relevant to environmental conditions and health standards in Indonesia. When compared with international guidelines, such as those established by the World Health Organization (WHO) and the United States Environmental Protection Agency (EPA), the thresholds used in this study were generally consistent with acceptable pollutant exposure levels, although international standards typically emphasize long-term exposure limits rather than short-term indoor monitoring. Based on these thresholds, the system automatically classified room conditions by comparing the measured sensor values to the predefined categories. The classification results were used to determine the safety status of the room and to trigger mitigation mechanisms, such as activating the exhaust fan at the main node, thereby ensuring timely response to potentially hazardous air quality conditions (Table 3).

Table 3. Threshold values classification.

Parameters	Safe Threshold	Danger Threshold
TVOC	< 200 ppb	> 200-500 ppb
eCO2	< 1000 ppm	> 1000-1500 ppm

3. Results and Discussion

3.1. Hardware implementation.

The hardware implementation stage began with the assembly of all main components according to the system design developed during the design stage. The devices used included the Wemos D1 Mini, ENS160 + AHT21 sensors, and the Orange Pi 4A as the main control unit for the air quality monitoring system. All components were assembled into a single interconnected circuit, ensuring stable communication lines, safe cable arrangement, and easy access to modules for testing and maintenance purposes. Each part was tested individually to verify that the basic functions worked correctly, including sensor readings, LCD display operation, power supply verification, and connectivity between modules. This approach was adopted to minimize failures during the overall system integration process. Figure 6 shows the complete hardware configuration of the developed system, including the main control unit, two distributed sensor nodes, and the exhaust ventilation actuator. This integrated configuration demonstrates the practical implementation of the proposed multi-node architecture for real-time indoor air quality monitoring and automatic mitigation.

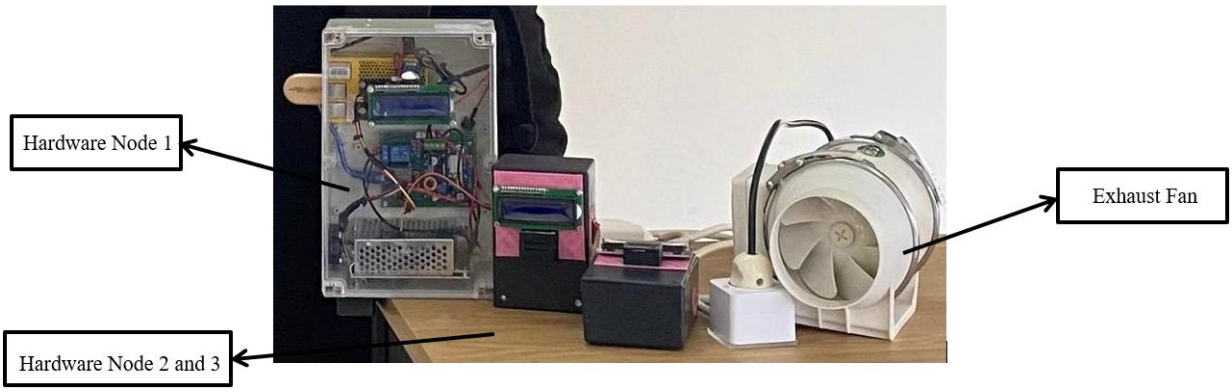

Figure 6. Hardware implementation of the air quality monitoring system.

Figure 7 presents detailed views of the individual nodes. Figure 7(a) shows the assembled main unit (Node 1), configured as the central monitoring and control device. The casing integrates the sensor, processing, and control modules into a single compact structure designed for fixed installation. Its physical layout ensured stable power distribution, structured cabling, and direct interfaces with actuators to support automated ventilation control. Figure 7(b) shows the distributed sensor nodes (Node 2 and Node 3), which were designed to be compact and portable. Their self-contained casings supported flexible placement at various monitoring points within the room. The modular design enhanced mobility and ease of deployment while maintaining consistent real-time data acquisition and wireless communication with the central gateway.

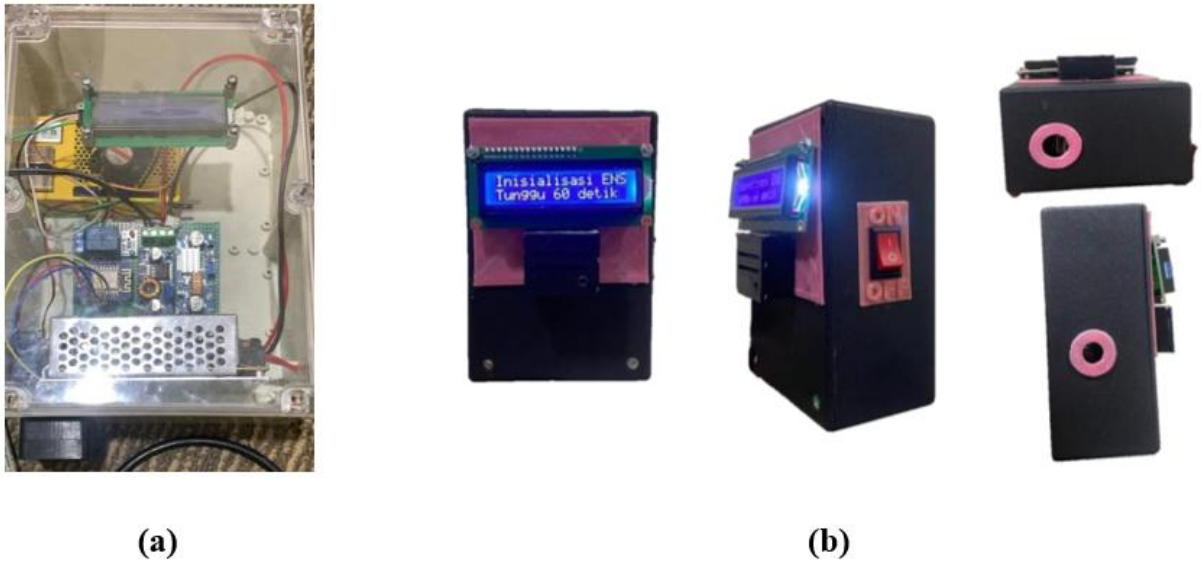

Figure 7. Hardware implementation of the air quality monitoring system: (a) Node 1 main unit (b) Node 2 and Node 3 sensor nodes.

3.2. Software implementation.

The Wemos D1 Mini microcontroller was programmed using Visual Studio Code (VS Code) with the ESP8266 development framework. The firmware was developed to read sensor data, process air quality measurements, and transmit the data in real time to the IoT platform via the MQTT communication protocol. The software implementation phase focused on developing firmware for each sensor node and configuring the IoT communication and visualization platform. The firmware initialized the ENS160 + AHT21 sensors, periodically read environmental parameters, and processed the obtained data before transmission. The measured parameters included Total Volatile Organic Compounds (TVOC), estimated CO_2 (eCO_2), temperature, and relative humidity. Each data reading was formatted into a structured JSON payload to ensure compatibility with the MQTT publish-subscribe communication model. Once formatted, the data were transmitted wirelessly to an MQTT broker hosted on the Orange Pi 4A. The transmitted data were then displayed on the Node-RED dashboard for real-time monitoring. Figure 8 presents the Node-RED dashboard interface implemented for monitoring indoor air quality parameters. The dashboard displays readings from multiple sensor nodes, including TVOC, eCO_2, temperature, and humidity values. Each parameter is visualized using gauge indicators and time-series graphs, facilitating intuitive interpretation of air quality

conditions. The interface also incorporates air quality classification indicators based on predetermined health thresholds. When pollutant concentrations exceeded safe limits, the dashboard provided visual warnings and triggered the exhaust fan control mechanism at Node 1.

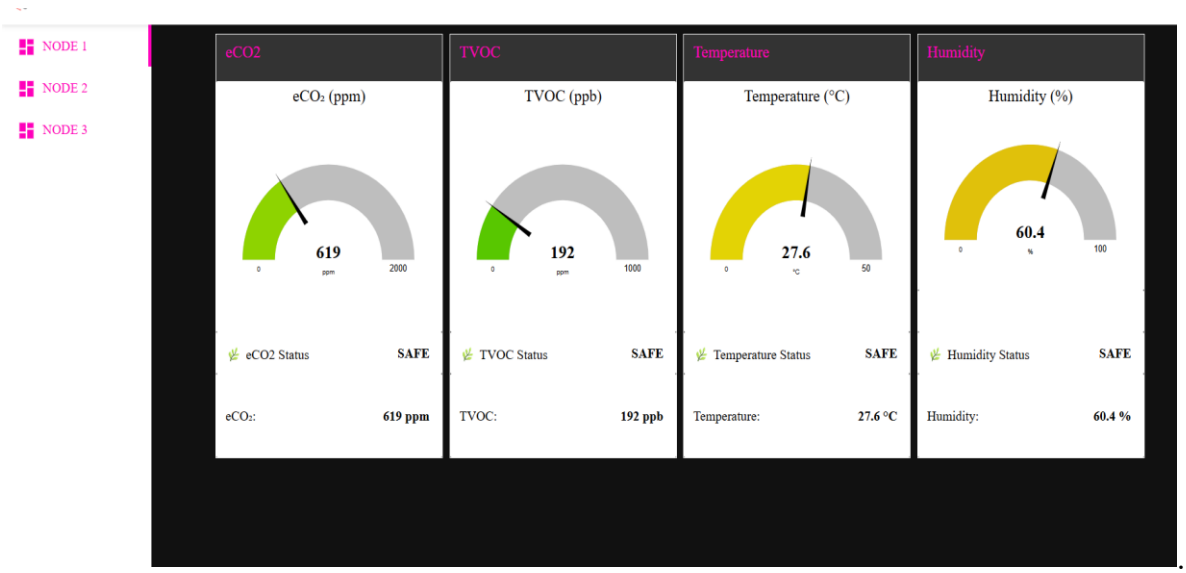

Figure 8. Dashboard display results.

3.3. System testing.

System testing was conducted to evaluate sensor response performance, measurement stability, and threshold classification capabilities, following the evaluation methods described in Sections 2.4 and 2.5. Data collection was performed automatically and transmitted via the MQTT protocol to the Orange Pi 4A server, then stored in a MySQL database for further analysis.

3.3.1. TVOC response test results.

The TVOC test results, based on the experimental scenarios described in Section 2.4, demonstrated a significant change in sensor response to pollutant exposure within the test chamber. The detected concentration profiles during the observation period are presented in Figure 9, which illustrates the dynamics of TVOC values over time, including patterns of increase, decrease, and fluctuations in sensor response during testing. Figure 9 shows the TVOC response trend under three different NH_3 concentration exposures: 100%, 50%, and 10%. The results indicated a clear concentration-dependent behavior of the ENS160 sensor. At an NH_3 concentration of 100%, a rapid and significant increase in TVOC values was observed immediately after exposure, followed by fluctuating peaks that suggested high VOC accumulation and a possible temporary sensor saturation effect. At a concentration of 50%, the TVOC response exhibited moderate peak levels with reduced variability compared to the 100% condition. Meanwhile, exposure to a concentration of 10% resulted in relatively stable and low TVOC readings, which remained within the safe threshold range.

.

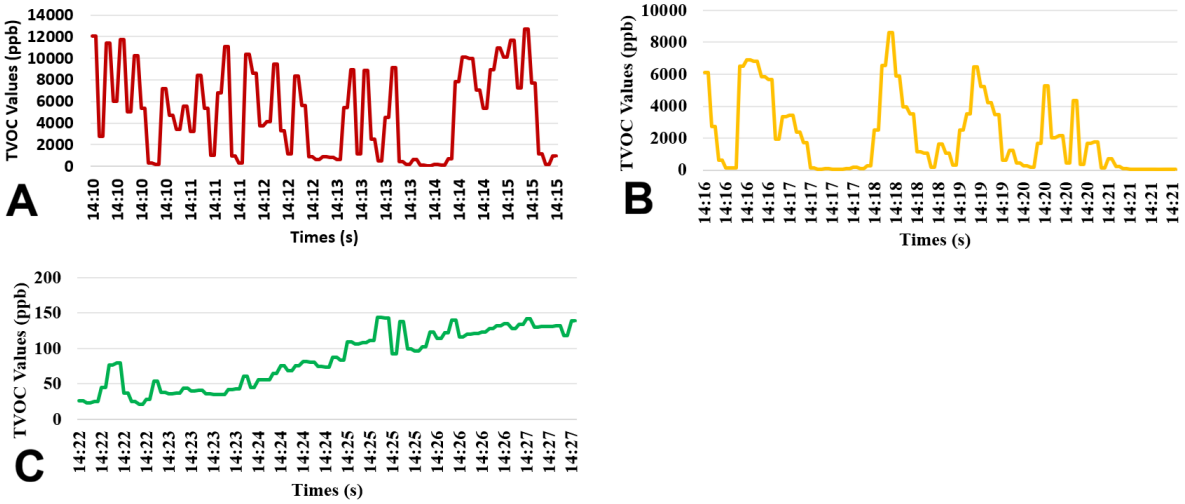

Figure 9. TVOC response under NH_3 exposure at different concentrations, (a) 100%, (b) 50%, (c) 10% NH_3.

TVOC testing using NH_3 solutions at concentrations of 100%, 50%, and 10% showed a clear concentration-dependent response pattern. At 100% exposure, TVOC values increased sharply, reaching a maximum of 12,697 ppb, with an average of 5,037 ppb and a standard deviation of 3,992 ppb, indicating high sensitivity but also considerable fluctuation at extreme concentrations. This behavior aligned with the working principle of metal-oxide semiconductor (MOX) sensors, where changes in gas concentration alter the resistance of the sensing material through surface redox reactions [11,12]. At 50% concentration, the TVOC range decreased to 33–8,605 ppb, with an average of 2,106 ppb and improved stability, demonstrating more consistent sensor performance at moderate exposure levels, as reported in previous MOX sensor studies [11]. At 10% exposure, TVOC values remained within 21–144 ppb (average 84 ppb), falling within the safe threshold and showing stable, low-variability responses consistent with prior IoT-based IAQ monitoring research [14]. Overall, the proportional increase in TVOC values with rising NH_3 concentration confirmed the concentration-dependent response characteristic of MOX sensors, although potential limitations, such as sensor drift and environmental sensitivity, should be considered when interpreting extreme readings. The detailed results are summarized in Table 4.

Table 4. TVOC test results.

No	Test material	Minimum TVOC (ppb)	Maksimum TVOC (ppb)	Average (ppb)	Standard deviation (±SD)
1.	Liquid NH3 100% concentration	67	12697	5037	3992
2.	Liquid NH3 50% concentration	33	8605	2106	2336
3.	Liquid NH3 10% concentration	21	144	84	40

3.3.2. eCO2 response test results.

The eCO_2 test results based on the experimental scenario described in Section 2.4 showed a significant change in sensor response to pollutant exposure within the test chamber. The detected concentration changes over time are illustrated in Figure 10, which shows the dynamics of eCO_2 values, including patterns of increase, decrease, and fluctuations in sensor response during the testing process. The eCO_2 response for exposure to cigarette smoke and air fresheners is presented in Figures 10(a) and 10(b), respectively. Both tests showed a pronounced temporary increase in estimated CO_2 levels immediately after the introduction of pollutants. When exposed to cigarette smoke, the sensor recorded a sharp spike, followed by

fluctuations in values as VOC compounds accumulated and dispersed within the semi-enclosed room. In contrast, exposure to air fresheners produced a noticeable peak that was relatively lower than that observed for cigarette smoke. This pattern indicated that the sensor's internal algorithm interpreted increases in VOC concentrations as corresponding increases in equivalent CO_2 levels, which is consistent with the operational characteristics of digital MOX-based air quality sensors [6].

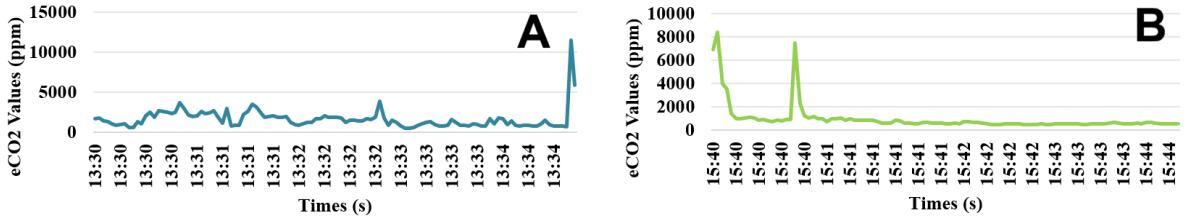

Figure 10. Estimated CO_2 (eCO_2) response during pollutant exposure, (a) cigarette smoke, (b) air freshener.

Statistical analysis presented in Table 5 showed that cigarette smoke exposure produced higher maximum and average eCO_2 values than air freshener exposure, reflecting the higher VOC concentration and chemical complexity of cigarette smoke. Similar behavior has been reported in previous studies, where MOX-based sensors exhibited elevated eCO_2 readings under high VOC exposure due to algorithm-based estimation mechanisms [11,12]. The relatively large standard deviation observed in both conditions indicated dynamic environmental fluctuations typical of semi-enclosed spaces with uneven pollutant dispersion. Since the ENS160 estimates eCO_2 indirectly from VOC levels, these values represented equivalent CO_2 rather than direct CO_2 measurements. Cigarette smoke, which contains complex reactive VOC compounds, generated higher peaks and variability compared to air fresheners, which mainly released alcohol- and ester-based compounds, resulting in lower average responses [11,12]. The experimental results further indicated that the ENS160 sensor exhibited a nonlinear response under high VOC exposure. At high NH_3 concentrations, the sensor showed rapid spikes followed by fluctuations, suggesting temporary saturation of the MOX sensing layer due to excessive gas adsorption, a behavior commonly reported in MOX sensors [11,12]. Higher standard deviation values at 100% and 50% concentrations reflected rapid pollutant accumulation and uneven gas distribution, while environmental factors such as humidity and temperature likely contributed to short-term variability. Nevertheless, the proportional decrease in mean values and variability at lower concentrations confirmed the sensor's ability to distinguish different pollutant intensity levels. For long-term operation, periodic calibration was recommended to minimize potential drift and maintain measurement accuracy [11,12].

Table 5. eCO2 test results.

No	Test material	Minimum eCO2 (ppm)	Maksimum eCO2 (ppm)	Average (ppm)	Standard deviation (±SD)
1.	Cigarette smoke	506	11524	1663	1245
2.	Air freshener	462	8452	959	1261

4. Conclusions

The developed system successfully monitored TVOC and estimated CO_2 (eCO_2) parameters in real time through MQTT communication and Node-RED visualization. Experimental results

showed that the ENS160 sensor exhibited a concentration-dependent response, where higher pollutant exposure resulted in higher sensor readings. Statistical evaluation using mean and standard deviation confirmed that the system consistently distinguished between different pollutant intensity levels with acceptable measurement stability. In addition, threshold-based classification, implemented in conjunction with automatic ventilation fan activation, enabled responsive mitigation of indoor air quality deterioration. Compared to previous IoT-based air quality monitoring implementations that primarily focused on single-node monitoring or notification systems, the proposed system provided a scalable multi-node architecture integrated with real-time control capabilities, supporting both monitoring and active environmental response. However, some limitations remained. The performance of MOX-based sensors was affected by environmental factors such as humidity and temperature, which could cause short-term variability. Long-term exposure to high VOC concentrations could also lead to sensor drift, while the eCO_2 parameter represented an algorithm-based estimate rather than a direct CO_2 measurement. The modular multi-node architecture enabled easy scalability for deployment across multiple rooms or industrial areas without major system modifications. Future developments may include the integration of additional sensors, such as particulate matter ($PM_{2.5}$/PM_{10}) and specific gas sensors, as well as the implementation of cloud-based predictive analytics to support early detection of air quality deterioration and proactive environmental control.

Acknowledgments

The authors expressed their sincere gratitude to all parties who supported the completion of this research. The authors also acknowledged the support from academic supervisors and colleagues for their valuable guidance, technical suggestions, and constructive feedback throughout the research process. Additionally, appreciation was given for the technical assistance and facilities provided during the development, implementation, and evaluation of the IoT-based indoor air quality monitoring system. This research did not receive any specific grant from funding agencies in the public, commercial, or not-for-profit sectors.

Competing Interest

The authors declared that there were no known competing financial or personal interests that could have appeared to influence the work reported in this paper.

Author Contributions

Siti Milda Alkan Dawasoka and Eka Puji Widiyanto contributed equally to this work. Both authors were involved in the conceptualization, methodology, formal analysis, software implementation, and manuscript writing.

References

[1] WHO Global Air Quality Guidelines: Particulate Matter (PM2.5 and PM10), Ozone, Nitrogen Dioxide, Sulfur Dioxide and Carbon Monoxide. (accessed on 1 December 2025) Available online: https://www.who.int/publications/i/item/9789240034228.

[2] Status Lingkungan Hidup Indonesia (SLHI) 2023, Jakarta, Indonesia, 2023. (accessed on 1 December 2025) Available online: https://www.menlhk.go.id.

[3] Nashira, A.; Nugrahani, A.P.; Rahmah, A.U.; Cahyono, T. (2025). Quantitative Risk Assessment of Ammonia Release from Storage Tanks Using RISKCURVES Software. *Engineering Proceedings*, *84*, 80. https://doi.org/10.3390/engproc2025084080.

[4] Nie, T.; Zhang, G.; Sun, Y.; Wang, W.; Wang, T.; Duan, H. (2025). Effects of Indoor Air Quality on Human Physiological Impact: A Review. *Buildings*, *15*, 1296. https://doi.org/10.3390/buildings15081296.

[5] Gorgoglione, A.; Bombardelli, F.A.; Pitton, B.J.L.; Oki, L.R.; Haver, D.L.; Young, T.M. (2018). Role of Sediments in Insecticide Runoff from Urban Surfaces: Analysis and Modeling. *International Journal of Environmental Research and Public Health*, *15*, 1464. https://doi.org/10.3390/ijerph15071464.

[6] DFRobot. *ENS160 Digital Multi-Gas Sensor Datasheet*, Shenzhen, China, 2023. [Online]. Available: https://wiki.dfrobot.com/ENS160_Air_Quality_Sensor_SKU_SEN0544.

[7] da Silva, A.H.M.C.; da Silva, M.K.; Santos, A.; Gómez-Malagón, L.A. (2025). A Systematic Review for Ammonia Monitoring Systems Based on the Internet of Things. *IoT*, *6*, 66. https://doi.org/10.3390/iot6040066.

[8] SparkFun ENS160 Air Quality Sensor Hookup Guide. (accessed on 1 December 2025) Available online: : https://learn.sparkfun.com/tutorials/ens160-air-quality-sensor-hookup-guide.

[9] Jo, J.H.; Jo, B.; Kim, J.H.; Choi, I. (2020). Implementation of IoT-Based Air Quality Monitoring System for Investigating Particulate Matter (PM_{10}) in Subway Tunnels. *International Journal of Environmental Research and Public Healt*, *17*, 5429. https://doi.org/10.3390/ijerph17155429.

[10] Mota, A.; Serôdio, C.; Briga-Sá, A.; Valente, A. (2025). Implementation of an Internet of Things Architecture to Monitor Indoor Air Quality: A Case Study During Sleep Periods. *Sensors*, *25*, 1683. https://doi.org/10.3390/s25061683.

[11] Flowerday, C.E.; Lundrigan, P.; Kitras, C.; Nguyen, T.; Hansen, J.C. (2023). Utilizing Low-Cost Sensors to Monitor Indoor Air Quality in Mongolian Gers. *Sensors*, *23*, 7721. https://doi.org/10.3390/s23187721.

[12] Spinelle, L.; Gerboles, M.; Kok, G.; Persijn, S.; Sauerwald, T. (2017). Review of Portable and Low-Cost Sensors for the Ambient Air Monitoring of Benzene and Other Volatile Organic Compounds. *Sensors*, *17*, 1520. https://doi.org/10.3390/s17071520.

[13] Yasin, M.; Nugroho, A.A.; Prasetyo, H. (2022). An IoT Framework for Indoor Air Quality Monitoring Using Commercial Sensors and Cloud-Based Visualization. *Applied Sciences*, *12*, 1–17. https://doi.org/10.3390/app12199450.

[14] Taştan, M.; Gökozan, H. (2019). Real-Time Monitoring of Indoor Air Quality Using Low-Cost IoT-Based Electronic Nose. *Applied Sciences*, *9*, 1–15. http://doi.org/10.3390/app9163435.

[15] Mota, L.; Silva, J.P.; Oliveira, R. (2025). An IoT-Based Indoor Air Quality Monitoring System Using ESP32-C6 and MQTT Protocol. *Sensors*, *25*, 1–18. http://doi.org/10.3390/s25061683.

[16] Shahid, S.; Brown, D.J.; Wright, P.; Khasawneh, A.M.; Taylor, B.; Kaiwartya, O. (2025). Innovations in Air Quality Monitoring: Sensors, IoT and Future Research. *Sensors*, *25*, 2070. http://doi.org/10.3390/s25072070.

[17] Garcia, A.; Saez, Y.; Harris, I.; Huang, X.; Collado, E. (2025). Advancements in Air Quality Monitoring: A Systematic Review of IoT-Based Air Quality Monitoring and AI Technologies. *Artificial Intelligence Review*, *58*, 275. http://doi.org/10.1007/s10462-025-11277-9.

[18] Zidni, H.; Putra, K.T.; Santosa, F.G.; Nugroho, A.; Pranoto, S.; Rahaman, M.; Chu, H.-T. (2024). Developing a Scalable IoT-Based Platform for Enhancing Air Quality Monitoring in Public Transport Using Node-RED. *Journal of Electrical Technology UMY*, *8*, 60–66. http://doi.org/10.18196/jet.v8i2.24701.

[19] Azizah, D.N.; Heranurweni, S.; Idris, L.O.M. (2025). Internet of Things Based Air Quality Monitoring System with Automatic Notification. *MALCOM: Indonesian Journal of Machine Learning and Computer Science*, *5*, 776–787. http://doi.org/10.57152/malcom.v5i3.1945.

[20] Kim, K.; Chun, D.; Yang, W. (2025). IoT-Based Filter Management System Using Reinforced ANFIS for VOCs Reduction in Urban Industrial Facilities. *Scientific Reports*, *15*, 17455. http://doi.org/10.1038/s41598-025-02435-8.

[21] Montgomery, D.C.; Runger, G.C. (2018). Applied Statistics and Probability for Engineers, 7th ed.; Wiley: Hoboken, NJ, USA.